

Balancing Constraints and Submodularity in Data Subset Selection

Srikumar Ramalingam Daniel Glasner Kaushal Patel Raviteja Vemulapalli Sadeep Jayasumana
Sanjiv Kumar
Google Research

{rsrikumar, dglasner, khpatel, ravitejavemu, sadeep, sanjivk}@google.com

Abstract

Deep learning has yielded extraordinary results in vision and natural language processing, but this achievement comes at a cost. Most deep learning models require enormous resources during training, both in terms of computation and in human labeling effort. In this paper, we show that one can achieve similar accuracy to traditional deep-learning models, while using less training data. Much of the previous work in this area relies on using uncertainty or some form of diversity to select subsets of a larger training set. Submodularity, a discrete analogue of convexity, has been exploited to model diversity in various settings including data subset selection. In contrast to prior methods, we propose a novel diversity driven objective function, and balancing constraints on class labels and decision boundaries using matroids. This allows us to use efficient greedy algorithms with approximation guarantees for subset selection. We outperform baselines on standard image classification datasets such as CIFAR-10, CIFAR-100, and ImageNet. In addition, we also show that the proposed balancing constraints can play a key role in boosting the performance in long-tailed datasets such as CIFAR-100-LT.

1. Introduction

Deep learning has shown unprecedented success in many domains, such as speech [25], computer vision [38, 59, 24], and natural language processing [58, 14]. This success generally relies on access to significant computational resources and large human-annotated datasets. For example, energy consumption and carbon footprint of developing common NLP models are shown to be comparable to the lifetime emissions of a car [57]. Similarly, human annotation is also a time-consuming and expensive process; [2] reports that semantic labeling of a single video frame takes around 45-60 minutes.

In this paper we ask the following question: Given a large unlabeled dataset along with a small labeled (seed) dataset and an annotation budget, how do we select a subset of

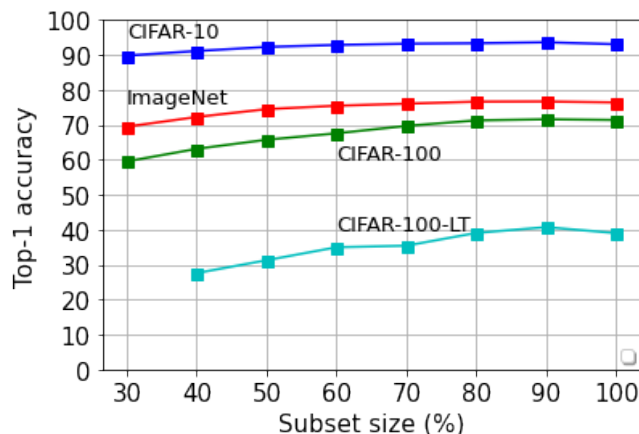


Figure 1: We show the accuracy of ResNet56 models trained on subsets of different sizes, selected using our method on CIFAR-10, CIFAR-100, ImageNet, and CIFAR-100-LT. Models trained using subsets with 30-40% less data, achieve similar accuracy to the ones trained using the full dataset.

the unlabeled dataset, which, when annotated, will achieve the best performance? While this is addressed by many classical active learning methods [54], in this work we focus on the modern deep learning setting with CNNs and very deep networks such as ResNets [24]. Typical active learning methods employ an iterative process where a single image is labeled and used to update the model at each step. The updated model is then used to pick the next image and so on. Such an approach is not feasible for deep networks. We therefore choose to study this problem in a batch setting [53].

In this setting, we start with a small random subset of 10% of the annotated data, which we refer to as a seed. The seed is used to train an initial model. After this, as done in the standard batch-mode active learning setup, our algorithm uses this initial seed model to select a subset of the full dataset for which the labels will be revealed. We then train a new model with the selected subset. As shown in Fig. 1, our subset selection methods can identify subsets with 30% to 40% less data, which achieve performance similar to what

we could get training with the full annotated dataset.

Most existing methods for data subset selection use some notion of *margin*, *representativeness*, or *diversity*. For example, the classical margin sampling selects images for which the prediction of the class labels are most uncertain. These could, for example, be the images having smallest difference between the highest and the second highest label probabilities [40]. Clustering-based objectives such as k-center [53] or k-medoids [30] select cluster centers with rich representativeness to model the entire dataset. Diverse subsets are identified by casting the problem as the maximization of submodular functions [63], which are discrete analogues of convex functions.

We see two main limitations with existing methods. First, there is no single subset selection criterion that achieves the best performance on different classification datasets. For example we observe in our experiments (Sec. 6) that in certain datasets, diversity works better than margin, and vice versa.

The second limitation is particularly relevant to margin-based methods where the selection is driven by the closeness of an image to the decision boundary. In a classification problem with L labels, we have $\binom{L}{2}$ decision boundaries. Most margin-based methods greedily select images close to the decision boundary. This often results in a selection of too many images representing a small number of boundaries, while ignoring many others.

To address the first limitation, we develop a unified algorithm based on maximization of a submodular function, which combines different selection objectives based on user-specified preferences. Importantly, we do this without sacrificing constant approximation guarantees. To address the second limitation, we incorporate class-balancing and boundary-balancing constraints in our optimization using intersection of matroids. In addition to addressing the two limitations, we also propose an improved diversity objective function. The diversity promoting objective functions typically use an underlying nearest neighbor graph that models the distances between the training samples. Specifically, our improved diversity objective function models the simultaneous interaction of three nearby samples, while the standard approach typically considers the interaction of two nearby samples.

To summarize, our contributions are: (1) We propose a general framework that unifies different subset selection algorithms. We further show that many popular data subset selection objectives can be cast as the maximization of submodular functions. As a result, we are able to provide constant approximation guarantees for our unified algorithm. (2) We model class-balancing and boundary-balancing constraints using matroids, and incorporate these constraints in the subset selection algorithm using intersection of matroids. We show that accounting for the balancing constraints leads to improved subsets. (3) We propose an improved diversity

objective function based on 3-clique interactions in the nearest neighbor graph. (4) We outperform baseline methods on standard classification datasets (CIFAR-10, CIFAR-100, and ImageNet) and long-tailed datasets such as CIFAR-100-LT.

2. Related Work

Data summarization and submodularity: Submodularity [45], often seen as the discrete analogue of convexity, can be used to model subset selection objectives associated with diversity and representativeness. While subset selection problems are mostly NP-hard, submodular optimization algorithms are efficient and come with constant approximation guarantees [8, 56, 36, 21, 63, 41, 31, 33, 48, 21, 22, 27, 66, 49, 12, 16].

A submodular function that promotes representativeness and diversity was utilized in document summarization [41]. Discriminant point process (DPP) are probabilistic models capable of selecting diverse subsets. They were used for minibatch selection in [43], and the maximum a posteriori (MAP) inference for DPP is submodular [9].

Uncertainty sampling and active learning: Active learning methods primarily focus on reducing the label annotation costs by selecting images to label that are more likely to yield the best model (See [53] for a detailed survey). Theoretical guarantees are usually about how quickly the version space, that maintains a set of good candidate classifiers, shrinks based on the availability of new data [13]. Uncertainty sampling selects the most challenging or uncertain images first, in the hope that this will eliminate the need to label other, easier ones. In a classification setting, predictions from the initial model can provide class probabilities that can help identify images with high uncertainty. Possibilities include simple uncertainty measures from the best and second best class probabilities [40, 51], entropy measure [26, 28], and geometric distance to the decision boundary [60, 7], selection via proxies [10], and query by committee [20, 55], where a committee of models are used to identify images where they most disagree.

Clustering and coresets: A coreset is a small set of points that approximates the shape of a larger point set. In an ML setting it is a small subset of images from a larger dataset such that the model trained on the coreset is competitive with the one learned from the entire dataset. It is shown in [53, 64] that the average loss over any given subset of the dataset and the remaining points can be bounded, and that the minimization of this bound can be mapped to the k-center problem. Other classical techniques for subset selection include clustering algorithms such as k-medoids [30, 47], which minimizes the sum of dissimilarities between images belonging to a cluster and a point designated as its center. Agglomerative clustering was used to select subsets in [5], where it was shown that at least 10% of images are redundant in ImageNet and CIFAR-10 training. In this work, we show

that at least 30-40% of the images in CIFAR-10, CIFAR-100 and ImageNet are redundant.

Learning prototypes and criticisms: In the context of interpretability, *prototypes* are subsets that best represent the entire dataset where a learned model performs the best, and *criticisms* are the images where a learned model does not do well. Both prototypes and criticisms can be modeled using maximum-mean discrepancy (MMD), that measures the difference between two distributions. The resulting optimization to compute the subsets can be cast as submodular maximization [33]. Minimization of the MMD between the entire dataset and the selected subset can be seen as empirical risk minimization, and such an approach was used for batch mode active learning [62]. Other classical techniques for prototype selection includes k-medoids [4].

3. Problem Statement and Roadmap

We consider a classification setting with L classes and n training images $\mathcal{U} = \{x_1, \dots, x_n\}$. Let $G = \{1, \dots, n\}$ denote the indices in the dataset. Let $\psi : \mathcal{X} \rightarrow \mathbb{R}^L$ be a (trained) neural network that maps an input image to a probability distribution over the L classes. The model ψ can be seen as the composition of an *embedding function* $\phi : \mathcal{X} \rightarrow \mathbb{R}^D$ that maps an input to an D -dimensional embedding, and a *discriminator function* $h : \mathbb{R}^D \rightarrow \mathbb{R}^L$ that maps the embedding to output probability predictions.

Subset selection and model evaluation. We assume that we are given a small, annotated subset of \mathcal{U} , which we refer to as the *seed dataset* (this is 10% of \mathcal{U} in our experiments). We use this seed dataset to train an initial model ψ^{seed} . Our goal is to use this initial model to select a subset S of G , subject to a given annotation budget, such that when the images in S are annotated we can get the best classification performance training a new model with them. To this end, using the seed model, we generate embeddings and predictions for all the input images in \mathcal{U} . Next, we construct a neighborhood graph (G, E) where E denotes the weighted set of edges associated with nearby training images in the embedding space \mathbb{R}^D . Our subset selection algorithm only depends on these embeddings, predictions, and the nearest-neighbor graph (G, E) . As in the standard active learning settings, we do not use the groundtruth labels in \mathcal{U} while selecting subsets.

For modeling subset selection, we employ a submodular set function $f : 2^G \rightarrow \mathbb{R}$ that provides a utility value for every subset of G using notions of uncertainty and diversity. We show that the class and boundary balancing constraints can be enforced using intersections of partition matroids. With this modeling, subset selection is essentially the task of finding the subset with maximum utility value while satisfying the matroid constraints. This inference problem is combinatorial in the number of training samples, and the brute-force solution is infeasible. For efficient inference, we

rely on the submodular property of the objective function and the use of matroids for modeling balancing constraints. Such an approach allows us to use an efficient greedy algorithm to maximize the objective function while satisfying matroid constraints with constant approximation guarantees.

Once the subset S is computed, we request the groundtruth labels for the images in S . We use the annotated subset $\mathcal{U}_S \subseteq \mathcal{U}$ to train a model ψ^S and evaluate its performance on a common held-out test set.

4. Background

In Sec. 5 we show that our subset selection objective is both submodular and monotonic. We formally define these properties of a set function below.

Definition 1. Let Ω be a finite set. A set function $F : 2^\Omega \rightarrow \mathbb{R}$ is **submodular** if for all $A, B \subseteq \Omega$ with $B \subseteq A$ and $e \in \Omega \setminus A$, we have $F(A \cup \{e\}) - F(A) \leq F(B \cup \{e\}) - F(B)$.

This property is also referred to as diminishing returns since the gain diminishes as we add elements [45].

Definition 2. A set function F is **monotonically non-decreasing** if $F(B) \leq F(A)$ when $B \subseteq A$.

In Sec. 5.1 we show how to incorporate class balancing and boundary balancing priors in the subset selection algorithm. We use algebraic structures called matroids and their intersections. We formally define them below.

Definition 3. A **matroid** is an ordered pair $M = (\Omega, \mathcal{I})$ consisting of a finite set Ω and a collection \mathcal{I} of subsets of Ω satisfying three conditions. (1) The collection contains the empty set, i.e., $\emptyset \in \mathcal{I}$. (2) If $I \in \mathcal{I}$ and $I' \subseteq I$, then $I' \in \mathcal{I}$. (3) If I_1 and I_2 are in \mathcal{I} and $|I_1| < |I_2|$, then there is an element e in $I_2 \setminus I_1$ such that $I_1 \cup \{e\} \in \mathcal{I}$.

The members of \mathcal{I} are called the independent sets of M . See [46] for other, equivalent definitions of matroids.

Definition 4. Let $\Omega_1, \dots, \Omega_n$ be a partition of the finite set Ω and let k_1, \dots, k_n be positive integers. The ordered pair $M = (\Omega, \mathcal{I})$ is a **partition matroid** if $\mathcal{I} = \{I : I \subseteq \Omega, |I \cap \Omega_i| \leq k_i, 1 \leq i \leq n\}$

Definition 5. Given two matroids $M_1 = (\Omega, \mathcal{I}_1)$ and $M_2 = (\Omega, \mathcal{I}_2)$ over the ground set Ω , the **intersection of the matroids** is given by $M_1 \cap M_2 = (\Omega, \mathcal{I}_1 \cap \mathcal{I}_2)$.

5. Subset Selection

We propose a unified formulation for different selection criteria for margin, diversity, and representativeness using set functions of the form $f : 2^G \rightarrow \mathbb{R}$, where 2^G is the power set of the vertex set G . Our formulation allows us

to i) fuse these different methods and ii) incorporate class- and boundary-balancing constraints. We further show that our unified objective function is submodular and monotonic, and that the balancing constraints could be incorporated as matroids (formally defined in Sec. 4). This implies that our efficient greedy algorithm comes with constant approximation guarantees [45].

We cast subset selection using a criterion f , as maximizing a corresponding set function under a budget constraint:

$$S^* = \arg \max_{S \subseteq G} f(S) \quad \text{s.t. } |S| = k. \quad (1)$$

Here S^* is the optimal subset based on the selection criterion, and k is the budget. Our functions consist of a sum of terms, and the individual terms are modeled using the distances between embeddings. These embeddings are produced by the initial model ψ^{seed} , which we train using the annotated seed dataset.

Our unified objective function is written as the conic combination of several individual functions based on uncertainty ($f_{\text{uncertainty}}$), diversity ($f_{\text{diversity}}$), clique function (f_{triple}), and maximum mean discrepancy (f_{mmd}):

$$f(S) = \lambda_1 f_{\text{uncertainty}}(S) + \lambda_2 f_{\text{diversity}}(S) + \lambda_3 f_{\text{triple}}(S) + \lambda_4 f_{\text{mmd}}(S), \quad (2)$$

where $\lambda_i \geq 0, i \in \{1, \dots, 4\}$. Each of these constituent functions have simple geometric interpretations (See Fig. 2), and we provide their analytical expressions below:

Uncertainty based sampling. We define the uncertainty-based utility function $f_{\text{uncertainty}}$ as:

$$f_{\text{uncertainty}}(S) = \sum_{i \in S} u(i), \quad (3)$$

where $u(i)$ is a utility value for each example $i \in G$, based on its uncertainty. There are three popular choices for the utility functions using uncertainty: least confident, margin [51], and entropy. In this paper, we use margin, which is applicable in a multi-class setting, and gives preference to “hard to classify” or “low margin” examples (see [51] for more details). More specifically:

$$u(i) = 1 - \left(P(Y = bb|x_i) - P(Y = sb|x_i) \right), \quad (4)$$

where bb and sb denote the best and the second best predicted class labels for x_i according to our initial model ψ^{seed} . $P(Y = \cdot | x_i)$ denotes the class probabilities predicted by the same model for x_i .

It has been shown that focusing on images from the decision boundary may not be sufficient, and that including images from higher density areas can be beneficial [29]. We therefore next consider other criteria that use pairwise and higher order interactions between images.

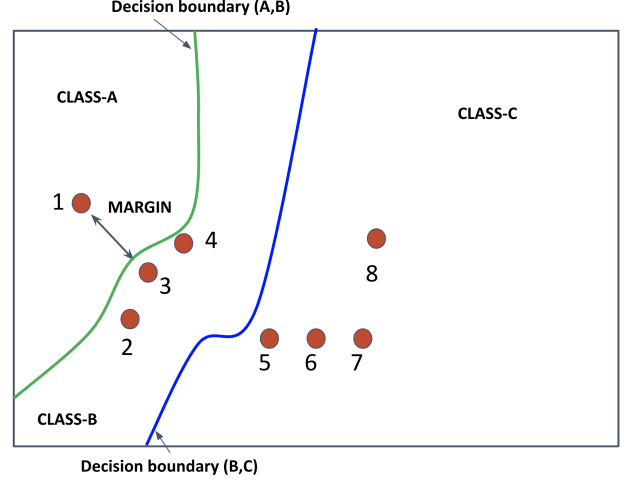


Figure 2: We show a toy scenario with three classes (A,B,C), 8 training samples, and two decision boundaries for the label pairs (A,B) and (B,C), respectively. The different objective functions have very simple geometric interpretations. For example, $f_{\text{diversity}}$ promotes selecting samples that are more spread out and thereby gives higher utility for $\{1, 3, 7\}$ over $\{2, 3, 4\}$. The uncertainty function $f_{\text{uncertainty}}$ prefers samples with high uncertainty or the ones closer to the decision boundary, and thus gives higher utility for $\{2, 3, 4\}$ over $\{1, 3, 7\}$. The clique function f_{triple} avoids selecting triplets with negligible or small area, and thereby gives very low utility for subsets such as $\{5, 6, 7\}$ where the samples all lie on a straight line. The f_{mmd} function on the other hand selects diverse points with high coverage, and thereby gives higher utility for set $\{3, 6\}$ over $\{1, 8\}$. The class balancing constraint would prefer a subset $\{1, 3, 7\}$, with samples from three classes, to a single class set $\{2, 3, 4\}$. Boundary-balancing constraint would prefer $\{4, 5\}$, which spans over two decision boundaries, to $\{3, 4\}$ lying near a single decision boundary.

Diversity. Given a budget on the size of the subset, the *diversity* criterion promotes selection of images that are diverse or spread apart in the embedding space. We define a set function $f_{\text{diversity}}$ that evaluates diversity as follows:

$$f_{\text{diversity}}(S) = \sum_{i \in S} \text{unary}(i) - \gamma \sum_{i,j: (i,j) \in E, i,j \in S} s(i,j). \quad (5)$$

The unary terms $\text{unary}(i)$ capture the utility of an individual image and the pairwise terms $s(i,j)$ are the similarity between a pair of images from the selected subset that have an edge $(i,j) \in E$ in the nearest neighbor graph (G, E) . As discussed in the Sec. 6, we use the cosine similarity in the embedding space as the similarity measure.

The hyperparameter $\gamma \geq 0$ determines the relative importance of the unary and pairwise terms. The pairwise term limits redundancy. If two points i and j with high similarity are both selected, we incur a penalty based on the similarity between them.

To ensure monotonicity of $f_{\text{diversity}}$, we can use a constant unary term, $\text{unary}(i) = \max_{l \in G} \sum_{j: (l,j) \in E} s(l, j)$.

Lemma 1. *The function $f_{\text{diversity}}$ is monotonically non-decreasing and submodular.*

The proof is available in the Appendix.

Clique function. Given a nearest neighbor graph, we identify cliques of size three by checking for edges among the k -nearest neighbors of every sample. Given a set of cliques given by \mathcal{T} , we define f_{triple} as follows:

$$f_{\text{triple}}(S) = \sum_{i \in S} \alpha(i) - \eta \sum_{i,j,k: (i,j,k) \in \mathcal{T}, i,j,k \in S} t(i, j, k). \quad (6)$$

where $\alpha(i)$ denotes the number of triple cliques involving the sample i , and $t(i, j, k)$ is 1 when the volume consumed by the embeddings of the triplet $\{i, j, k\}$ is less than a threshold $\mathcal{T}_{\text{thresh}}$, and 0 otherwise. The volume computation in higher dimensional space involves outer product [42], similar to cross-product in 3-dimensional space. For computational efficiency, we approximate the volume using the area of triangle based on the three side lengths obtained from the nearest neighbor graph. We can extend the idea of triple cliques to higher orders [34, 35], but this can be computationally expensive when we consider millions of training samples.

We prove the following lemma in the Appendix.

Lemma 2. *The function f_{triple} is monotonically non-decreasing and submodular.*

Maximum mean discrepancy. A variant of $f_{\text{diversity}}$ which promotes selection of images that are both representative and diverse can be obtained by defining unary terms that give preference to images with high coverage or connectivity. A subset is considered to have high coverage if its elements are closer to most or all the elements in the dataset.

$$f_{\text{mmd}}(S) = \sum_{i \in S} \sum_{j: (i,j) \in E} s(i, j) - \xi \sum_{i,j: (i,j) \in E, i,j \in S} s(i, j). \quad (7)$$

Here the first term promotes coverage, while the second promotes diversity. We refer to this as ‘‘MMD’’ since it is derived in [33] using a maximum mean discrepancy measure. We prove the following lemma in the Appendix.

Lemma 3. *The function f_{mmd} is monotonically non-decreasing and submodular.*

We note that there are other ways to maximize the diversity function. For example, by replacing the similarity term $s(i, j)$ with a metric distance function, the diversity criteria can be seen as the max-sum k diversification problem, for which algorithms exist with constant approximation guarantees [6].

Any conic combination of submodular functions is submodular [45], and thus $f(S)$ is submodular.

5.1. Balancing constraints

In this section we show how we incorporate balancing constraints in our unified formulation.

Class balancing constraint. Subsets selected based on diversity or margin criteria can lead to severe class imbalance. Consequently, models trained using these imbalanced subsets can show superior performance on common classes, and inferior performance on rare classes [11]. A reweighted loss function can partially address this problem but performance on classes with no, or very few representatives will still suffer.

To overcome this problem we incorporate explicit class-balancing constraints in our formulation. We do this using a partition matroid constraint, a choice that allows us to maintain our approximation guarantees. Consider a partition $\{G_1, G_2, \dots, G_L\}$ of the full dataset G . Here L denotes the number of classes and G_i consists of the images belonging to class i , where pseudo-labels are computed using the initial (seed) model. Let k_1, \dots, k_L be user-defined positive integers specifying the sizes of the desired subsets. We choose subsets that are independent sets of the partition matroid $M = (G, \mathcal{I}_p)$:

$$\mathcal{I}_c = \{I : I \subseteq G, |I \cap G_i| \leq k_i, 1 \leq i \leq L\}. \quad (8)$$

Boundary balancing constraint. The initial model $\psi^{\mathcal{I}}$ that we trained using the seed dataset, defines a set of decision boundaries for every pair of classes. Formally, the decision boundary for a pair of classes $\{a, b\}$ is given by:

$$\mathcal{D}_{\{a,b\}} \triangleq \{x; P(Y = a|x) = P(Y = b|x)\}, \quad (9)$$

where $P(y|x)$ are the posterior probabilities from the seed model. In other words, these are the set of points where the posterior class probabilities for two different classes agree. Decision boundaries can be defined in input space, output space, or in the space defined by the intermediate layers in the network [17]. Since we are only interested in associating an image to its closest decision boundary, our formulation does not require computation of the exact distance to the boundary. Instead we simply use predicted class probabilities.

We define the *margin score* of an image x_i (given predictions from the initial model) as

$$m(x_i) = 1 - (P(Y = bb|x_i) - P(Y = sb|x_i)), \quad (10)$$

where bb and sb correspond to best and the second best class labels, respectively. We associate x_i with the boundary (bb, sb) if $m(x_i) > \tau$, for some threshold τ .

We observe that the number of class boundaries grows quadratically with the number of classes and conjecture that

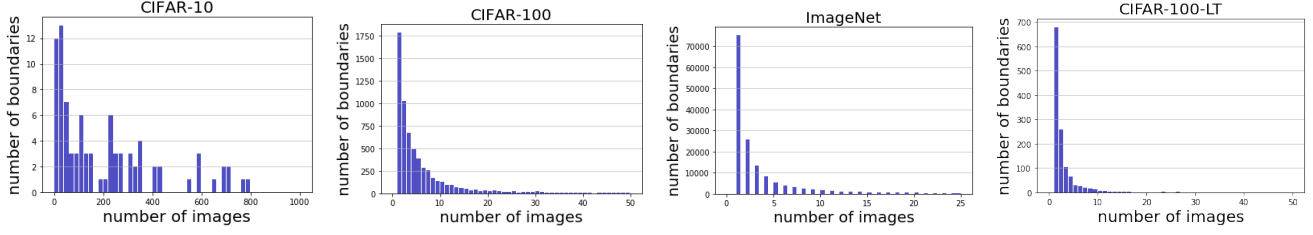


Figure 3: Histogram of the number of images associated with the class boundaries in CIFAR-10, CIFAR-100, ImageNet, and CIFAR-100-LT datasets.

many datasets with a large number of classes do not contain any images close to many decision boundaries. Our goal is to design a subset selection algorithm that promotes selection of images near as many decision boundaries as possible.

To quantify this observation, we use predictions from our initial model for ImageNet to associate any image in the dataset which has a margin score greater than $\tau = 0.05$ to the corresponding class boundary. Since ImageNet has 1000 classes, we have $\binom{1000}{2}$ boundaries. We found that 15% of all possible boundaries were covered.

Let $\mathcal{D} = \{b(x); x \in \mathcal{U}\}$ denote the set of all the decision boundaries associated with all the images in the training set \mathcal{U} , and $b(x)$ is a function that associates a given image to a certain decision boundary or to the empty set \emptyset , based on the margin score. In Fig. 3, we show the histogram of the number of images associated with different decision boundaries. We note that it is possible to associate an image to multiple decision boundaries, and defer exploring this option to future work.

Similar to the class-balancing problem, we consider a partition $\{G_{b_1}, G_{b_2}, \dots, G_{b_M}\}$ of the full dataset G , where G_{b_i} denotes the set of images belonging to the decision boundary $b_i \in \mathcal{D}$.

Let d_1, \dots, d_M be user-defined positive integers specifying the maximum number of images near different boundaries. Let us consider the following partition matroid $M = (G, \mathcal{I}_d)$:

$$\mathcal{I}_d = \{I : I \subseteq G, \quad |I \cap G_{b_i}| \leq d_i, 1 \leq i \leq M\} \quad (11)$$

In order to impose both class-balancing and boundary-balancing constraints, our selected subset should be the independent set of both the partition matroids given by (G, \mathcal{I}_c) and (G, \mathcal{I}_d) .

Note that the intersection of two matroids is not a matroid in general. However, [19] shows that applying the greedy algorithm to a submodular monotonic objective with matroid intersection constraints maintains approximation guarantees.

5.2. Greedy Algorithm

Subset selection using class- and boundary-balancing constraints is given by:

$$S^* = \arg \max_{S \subseteq G} f(S) \quad \text{s.t. } |S| = k, S \in \mathcal{I}_c, S \in \mathcal{I}_d, \quad (12)$$

where f is our unified objective. The greedy algorithm for selecting a subset of size k is given in Algorithm 1.

Algorithm 1: Greedy algorithm

1. Initialize $S = \emptyset$;
 2. Let $s = \arg \max_{s' \in G} f(S \cup \{s'\}) - f(S)$ such that $S \cup \{s'\} \in \mathcal{I}_c \cap \mathcal{I}_d$;
 3. If $s \neq \emptyset$ and $|S| < k$ then $S = S \cup \{s\}$, go to 2.;
 4. S is the required solution;
-

Given that f is monotonic and submodular, a theorem from [19] implies that we have a constant approximation guarantee for the greedy algorithm according to the bound $f(S_{\text{greedy}}) \geq \frac{1}{p+1} f(S_{\text{OPT}})$, where $f(\emptyset) = 0$ and p is the number of matroid constraints. Since we have two matroids, we have $f(S_{\text{greedy}}) \geq \frac{1}{3} f(S_{\text{OPT}})$.

6. Experiments

Datasets. We evaluate the performance of different subset selection methods for classification, using four datasets: CIFAR-10 [37], CIFAR-100 [37], ImageNet [50], and CIFAR-100-LT [44]. The last one is a long-tailed dataset where the head class is 100 times more frequent than the least-frequent class [44]. We include this dataset to demonstrate capabilities of our algorithm when there is severe class imbalance in the dataset. We do not apply any long-tail classification techniques as we want to compare the performance of vanilla ERM across different subset selection methods.

Initial model. For each of the datasets we select a random seed subset of size 10% and use it to train a ResNet-56 [24] initial model. We use the initial model to generate predictions and embeddings for all the images in the dataset. The embeddings are 64, 64, and 2048-dimensional vectors

for CIFAR-10, CIFAR-100, CIFAR-100-LT, and Imagenet, respectively. We construct the neighborhood graph (G, E) by finding the $k = 10$ nearest neighbors of each image in embedding space, using the fast similarity search of [23]. We evaluated different similarity measures such as cosine similarity, L_1 , and L_2 distances, and found no significant differences. All the reported experiments use cosine similarities.

Hyperparameters. For the CIFAR-10, CIFAR-100, and CIFAR-100-LT experiments we used 450 epochs and the learning rate is divided by 10 at the following epochs: 15, 200, 300, and 400. The base learning rate was set to 1.0. For ImageNet we used 90 epochs and the learning rate is divided by 10 at the following epochs: 5, 30, 60, and 80. The base learning rate was set to 1.5. In all the datasets, we used SGD with momentum 0.9 (with nestrov) for training. When trained with the full training set, the top-1 accuracies for CIFAR-10, CIFAR-100, ImageNet, and CIFAR-100-LT are 93.04%, 71.37%, 76.39%, and 39.01%, respectively. We use the same standard settings for all the experiments. To keep our experimental setup relatively simple, we do not include all of the bells and whistles, such as mixup [65] or semi-supervised learning [3] employed by the most competitive methods.

Evaluation. We show 4 subset selection methods as baselines: random, diversity, margin, and k-center [53]. The parameters (k_1, \dots, k_L) in the class-balancing partition matroid are set based on the desired subset size. In other words, k_i sets an upper limit on the number of images from a specific class. In our experiments, we set this value to be $\frac{\eta n}{L}$, where n , η , and L denote the number of images, fraction of the training set, and the number of labels, respectively. In the case of boundary balancing matroid, we set the parameters d_i to be $\max(1, \eta n_i)$, where n_i denotes the number of images associated with the decision boundary $b_i \in \mathcal{D}$. For each subset selection method and subset size, after selecting the subset, we reveal its labels and retrain a model on the annotated subset. Accuracy of this model is then reported on the standard test set. We show results on different size subsets in Tables 1, 2, 3, and 4.

The proposed method outperforms competing algorithms in class-balanced datasets such as CIFAR-10, CIFAR-100, and ImageNet. We observe larger gains in the long-tailed dataset, CIFAR-100-LT. Note that, on this dataset, accuracies with 80% and 90% subsets exceed that with the full dataset (see Table 4). This is not surprising since completely eliminating some examples in the training set has shown to be beneficial for long-tailed dataset [39, 61].

One striking aspect of this active learning experiment is that the gap between different sampling strategies is usually not that large. We are not the first to observe this behaviour. A very recent work [1] observed the same, and also showed that diversity induced by even random sampling can

sometimes produce better subsets than graph-based coresampling algorithms based on k-center [53].

Another intriguing behaviour that we may notice is that the subsets with 80% or 90% budget consistently outperform the models trained with the full dataset. Such bumps in the performance produced by almost full subsets have also been observed before [52].

Ablation study: Balancing constraints. In CIFAR datasets, the balancing constraints provide a marginal improvement of 0.61%. In CIFAR-100-LT, the balancing constraints provide a marginal improvement of 2.83%. The marginal utility is computed by taking the average improvement with and without the balancing constraints.

Ablation study: Clique function. In CIFAR datasets, the clique function produces a marginal improvement of 0.49%. In the long-tail CIFAR-100-LT dataset, we obtain a marginal improvement of 1.13%. The marginal utility is computed by taking the average improvement produced with and without the clique function.

Ablation study: Number of nearest neighbors. We evaluated the role of k , the number of nearest neighbors in kNNs. While we used $k = 10$ in all our experiments the marginal benefit in using $k = 100$ and $k = 1000$ are given by +0.15% and +0.25%, respectively.

Visualization of subsets. Fig. 4 shows a visualization of subsets of CIFAR-10 using different objective functions. We can see that the uncertainty based method (Fig. 4c) encourages selection of points close to decision boundaries. On the other hand k-center and diversity lead to more diverse selections. Comparing Figs. 4a and 4b we can see the effect of the representativeness promoting unary term employed by MMD.

Computational benefits: Note that we use the same number of epochs for all the experiments, so a model trained with a 50% subset will go through 50% of the steps compared to training using the full dataset. After accounting for the one-time overhead of training the seed model and computing the neighborhood graph, in places where we use 70% subsets and achieve similar performance as the entire dataset, we are saving computational resources without losing performance.

7. Discussion

In this work we introduce a unified framework that allows us to combine different selection criteria and to impose class and boundary balancing constraints. Our experiments using these new capabilities have led to interesting findings: (1) It was recently reported in [53] that many classical techniques such as entropy methods [28] are not effective on CNNs and large-scale datasets. In our findings, we observe that classical uncertainty based methods are still highly competitive to more recent methods such as k-center [53]. (2) Incorporating boundary balancing constraints usually leads to better subsets, and the benefit is highly prominent in long-tailed

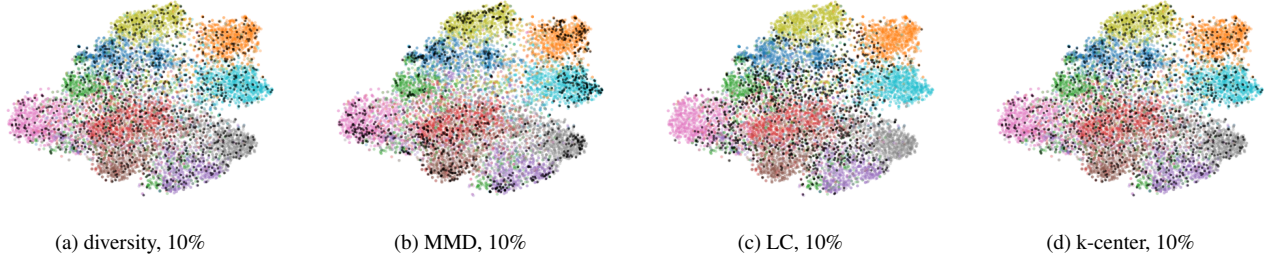


Figure 4: Visualization of different criteria. We show t -SNE projections of 10% subsets chosen using different criteria on CIFAR-10. Each of the 10 classes is represented with a different color. The selected images are in black.

%	random	margin	diversity	k-ctr	Ours
30	58.03	58.88	57.93	58.06	59.29
40	61.05	61.81	61.78	62.74	63.35
50	64.81	65.36	65.05	64.86	65.79
60	66.26	67.03	66.32	67.72	68.19
70	67.47	69.16	68.84	69.49	69.43
80	69.59	69.47	69.75	69.74	71.15
90	70.75	71.41	70.06	71.50	72.09
100	71.37	71.37	71.37	71.37	71.37

Table 1: Top-1 accuracy in % on CIFAR-100 dataset [37]. Our method outperforms the baselines on all budgets, except one.

%	random	margin	diversity	k-ctr	Ours
30	85.24	89.33	89.16	89.27	89.78
40	88.57	90.11	90.49	90.79	91.09
50	90.70	91.01	91.44	91.36	92.26
60	90.78	92.03	91.86	92.61	92.27
70	92.23	92.04	92.05	93.23	92.94
80	92.33	92.81	92.96	92.71	93.45
90	92.62	93.06	92.82	92.86	93.28
100	93.04	93.04	93.04	93.04	93.04

Table 2: Top-1 accuracy in % on CIFAR-10 dataset [37]. Our method outperforms the baselines under all budgets, except in two budgets.

datasets such as CIFAR-100-LT. (3) The use of clique function produces improvement over solely pairwise diversity functions. (4) Some popular image classification datasets have at least 30-40% redundant images, and it is possible to learn similar, or even slightly more accurate models with appropriate subsets.

We observe that subsets sometimes produce modest improvement over models trained with the full dataset. This makes us wonder if the monotonicity assumption on the

%	random	margin	diversity	k-ctr	Ours
30	65.02	67.64	67.60	67.32	68.67
40	68.92	71.45	70.95	70.98	71.86
50	70.86	73.41	72.95	72.51	74.28
60	72.39	74.70	74.26	74.78	75.37
70	72.92	75.57	75.40	75.62	76.11
80	74.36	75.39	76.02	76.26	76.73
90	75.10	76.11	76.30	76.02	76.63
100	76.39	76.39	76.39	76.39	76.39

Table 3: Top-1 accuracy in % on ImageNet dataset [50]. Our method outperforms all other baselines under all budgets.

%	random	margin	diversity	k-ctr	Ours
40	24.33	23.75	23.73	26.82	27.57
50	26.77	25.38	28.37	28.61	31.25
60	27.55	28.32	30.48	32.56	34.96
70	35.33	33.34	34.66	33.61	35.41
80	36.77	36.85	35.36	34.16	39.06
90	36.88	36.63	39.61	36.67	40.71
100	39.01	39.01	39.01	39.01	39.01

Table 4: Top-1 accuracy in % on CIFAR-100-LT dataset [37]. We significantly outperform all other baselines under all budgets.

utility function is a valid one. We plan to relax this assumption in future work, and explore non-monotonic approaches [18]. Other avenues of exploration include mini-batch selection [32] and modeling the submodular function as a differentiable layer in deep networks for end-to-end training [15].

Acknowledgement

We thank Chen Wang, Ramin Zabih, Aditya Menon, Hossein Mobahi, Dilip Krishnan, Xin Yu, and Sophia Domokos for valuable feedback.

References

- [1] Jordan T. Ash, Chicheng Zhang, Akshay Krishnamurthy, John Langford, and Alekh Agarwal. Deep batch active learning by diverse, uncertain gradient lower bounds, 2020. 7
- [2] V. Badrinarayanan, F. Galasso, and R. Cipolla. Label propagation in video sequences. In *CVPR*, 2010. 1
- [3] David Berthelot, Nicholas Carlini, Ian Goodfellow, Nicolas Papernot, Avital Oliver, and Colin Raffel. Mixmatch: A holistic approach to semi-supervised learning, 2019. 7
- [4] J. Bien and R. Tibshirani. Prototype selection for interpretable classification. *The Annals of Applied Statistics*, 2011. 3
- [5] V. Birodkar, H. Mobahi, and S. Bengio. Semantic redundancies in image-classification datasets: The 10% you don’t need, 2019. 2
- [6] A. Borodin, A. Jain, H. C. Lee, and Y. Ye. Max-sum diversification, monotone submodular functions, and dynamic updates. *ACM Trans. Algorithms*, 2017. 5
- [7] K. Brinker. Incorporating diversity in active learning with support vector machines. In *ICML*, 2003. 2
- [8] J. Carbonell and J. Goldstein. The use of mmr, diversity-based reranking for reordering documents and producing summaries. *SIGIR ’98*, 1998. 2
- [9] L. Chen, G. Zhang, and H. Zhou. Fast greedy map inference for determinantal point process to improve recommendation diversity. In *NeurIPS*, 2018. 2
- [10] C. Coleman, C. Yeh, S. Mussmann, B. Mirzasoleiman, P. Bailis, P. Liang, J. Leskovec, and M. Zaharia. Selection via proxy: Efficient data selection for deep learning, 2020. 2
- [11] Y. Cui, M. Jia, T. Y. Lin, Y. Song, and S. Belongie. Class-balanced loss based on effective number of samples. In *CVPR*, 2019. 5
- [12] Abhimanyu Das and David Kempe. Approximate submodularity and its applications: Subset selection, sparse approximation and dictionary selection. *Journal of Machine Learning Research*, 19(3):1–34, 2018. 2
- [13] S. Dasgupta, D. J. Hsu, and C. Monteleoni. A general agnostic active learning algorithm. In *NeurIPS*, 2008. 2
- [14] J. Devlin, M. W. Chang, K. Lee, and K. Toutanova. BERT: pre-training of deep bidirectional transformers for language understanding. *CoRR*, 2018. 1
- [15] J. Djolonga and A. Krause. Differentiable learning of submodular models. *NIPS*, 2017. 8
- [16] E. Elhamifar. Sequential facility location: Approximate submodularity and greedy algorithm. In *ICML*, 2019. 2
- [17] G. F. Elsayed, D. Krishnan, H. Mobahi, K. Regan, and S. Bengio. Large margin deep networks for classification. In *NIPS*, 2018. 5
- [18] U. Feige, V. S. Mirrokni, and J. Vondrak. Maximizing non-monotone submodular functions. In *FOCS*, 2007. 8
- [19] M.L. Fisher, G.L. Nemhauser, and L.A. Wolsey. An analysis of approximations for maximizing submodular set functions-ii. In *Polyhedral Combinatorics. Mathematical Programming Studies*, 1978. 6
- [20] R. Gilad-Bachrach, A. Navot, and N. Tishby. Query by committee made real. In *NIPS*, 2005. 2
- [21] Daniel Golovin and Andreas Krause. Adaptive submodularity: Theory and applications in active learning and stochastic optimization, 2010. 2
- [22] D. Golovin and A. Krause. Adaptive submodularity: Theory and applications in active learning and stochastic optimization. *J. Artif. Int. Res.*, 2011. 2
- [23] R. Guo, P. Sun, E. Lindgren, Q. Geng, D. Simcha, F. Chern, and S. Kumar. Accelerating large-scale inference with anisotropic vector quantization. In *ICML*, 2020. 7
- [24] K. He, X. Zhang, S. Ren, and J. Sun. Deep residual learning for image recognition. In *CVPR*, 2016. 1, 6
- [25] G. Hinton, L. Deng, G.E. Dahl, A. Mohamed, N. Jaitly, A. Senior, V. Vanhoucke, P. Nguyen, T. Sainath, and B. Kingsbury. Deep neural networks for acoustic modeling in speech recognition. *IEEE Signal Processing Magazine*, 2012. 1
- [26] A. Holub, P. Perona, and M. C. Burl. Entropy-based active learning for object recognition. In *CVPR Workshop*, 2008. 2
- [27] K J Joseph, Vamshi Teja R, Krishnakant Singh, and Vineeth N Balasubramanian. Submodular batch selection for training deep neural networks, 2019. 2
- [28] A. J. Joshi, F. Porikli, and N. Papanikolopoulos. Multi-class active learning for image classification. In *CVPR*, 2009. 2, 7
- [29] M. Karzand and R. D. Nowak. Active learning in the overparameterized and interpolating regime. *CoRR*, 2019. 4
- [30] L. Kaufman and P. J. Rousseeuw. Clustering by means of medoids, 1987. 2
- [31] V. Kaushal, R. Iyer, S. Kothawade, R. Mahadev, K. Doctor, and G Ramakrishnan. Learning from less data: A unified data subset selection and active learning framework for computer vision, 2019. 2
- [32] K. Kawaguchi and H. Lu. Ordered sgd: A new stochastic optimization framework for empirical risk minimization, 2019. 8
- [33] B. Kim, R. Khanna, and O. Koyejo. Examples are not enough, learn to criticize! criticism for interpretability. In *NIPS*, 2016. 2, 3, 5
- [34] P. Kohli, M. P. Kumar, and P. H. S. Torr. P3 beyond: Solving energies with higher order cliques. In *2007 IEEE Conference on Computer Vision and Pattern Recognition*, 2007. 5
- [35] V. Kolmogorov and R. Zabini. What energy functions can be minimized via graph cuts? *IEEE Transactions on Pattern Analysis and Machine Intelligence*, 26(2):147–159, 2004. 5
- [36] Andreas Krause and Daniel Golovin. Submodular function maximization. 2
- [37] Alex Krizhevsky et al. Learning multiple layers of features from tiny images. 2009. 6, 8
- [38] A. Krizhevsky, I. Sutskever, and G. E. Hinton. Imagenet classification with deep convolutional neural networks. In *NeurIPS*, 2012. 1
- [39] Miroslav Kubat and Stan Matwin. Addressing the curse of imbalanced training sets: One-sided selection. In *Proceedings of the International Conference on Machine Learning (ICML)*, 1997. 7
- [40] D. D. Lewis and W. A. Gale. A sequential algorithm for training text classifiers. In *SIGIR*, 1994. 2
- [41] H. Lin and J. Bilmes. A class of submodular functions for document summarization. In *ACL*, 2011. 2

- [42] Douglas Lundholm and Lars Svensson. Clifford algebra, geometric algebra, and applications, 2009. [5](#)
- [43] Z. Mariet, J. Robinson, J. Smith, S. Sra, and S. Jegelka. Optimal batch variance with second-order marginals. In *ICML Workshop*, 2020. [2](#)
- [44] Aditya Krishna Menon, Sadeep Jayasumana, Ankit Singh Rawat, Himanshu Jain, Andreas Veit, and Sanjiv Kumar. Long-tail learning via logit adjustment, 2020. [6](#)
- [45] G. L. Nemhauser, L. A. Wolsey, and M. L. Fisher. An analysis of the approximations for maximizing submodular set functions. *Mathematical Programming*, 1978. [2](#), [3](#), [4](#), [5](#)
- [46] James Oxley. *Matroid Theory*. Oxford University Press, 1992. [3](#)
- [47] H.S. Park and C.H. Jun. A simple and fast algorithm for k-medoids clustering. *Expert Systems with Applications*, 2009. [2](#)
- [48] A. Prasad, S. Jegelka, and D. Batra. Submodular meets structured: Finding diverse subsets in exponentially-large structured item sets. In *NIPS*, 2014. [2](#)
- [49] Chao Qian, Jing-Cheng Shi, Yang Yu, Ke Tang, and Zhi-Hua Zhou. Subset selection under noise. In I. Guyon, U. V. Luxburg, S. Bengio, H. Wallach, R. Fergus, S. Vishwanathan, and R. Garnett, editors, *Advances in Neural Information Processing Systems*, 2017. [2](#)
- [50] O. Russakovsky, J. Deng, H. Su, Krause J, S. Satheesh, S. Ma, Z. Huang, A. Karpathy, A. Khosla, M. Bernstein, A. C. Berg, and L. Fei-Fei. Imagenet large scale visual recognition challenge, 2014. [6](#), [8](#)
- [51] T. Scheffer, C. Decomain, and S. Wrobel. Active hidden markov models for information extraction. In *Advances in Intelligent Data Analysis*, 2001. [2](#), [4](#)
- [52] Greg Schohn and David Cohn. Less is more: Active learning with support vector machines. In *Proceedings of the Seventeenth International Conference on Machine Learning, ICML '00*, page 839–846, San Francisco, CA, USA, 2000. Morgan Kaufmann Publishers Inc. [7](#)
- [53] O. Sener and S. Savarese. Active learning for convolutional neural networks: A core-set approach, 2017. [1](#), [2](#), [7](#)
- [54] B. Settles. Active learning literature survey. Technical report, University of Wisconsin-Madison, 2009. [1](#)
- [55] H. S. Seung, M. Oppor, and H. Sompolinsky. Query by committee. In *COLT*, 1992. [2](#)
- [56] I. Simon, N. Snavely, and S. M. Seitz. Scene summarization for online image collections. In *ICCV*, 2007. [2](#)
- [57] E. Strubell, A. Ganesh, and A. McCallum. Energy and policy considerations for deep learning in NLP. *CoRR*, 2019. [1](#)
- [58] I. Sutskever, O. Vinyals, and Q.V. Le. Sequence to sequence learning with neural networks. In *NeurIPS*, 2014. [1](#)
- [59] C. Szegedy, W. Liu, Y. Jia, P. Sermanet, S. Reed, D. Anguelov, D. Erhan, V. Vanhoucke, and A. Rabinovich. Going deeper with convolutions. In *CVPR*, 2015. [1](#)
- [60] S. Tong and D. Koller. Support vector machine active learning with applications to text classification. *JMLR*, 2002. [2](#)
- [61] B.C. Wallace, K.Small, C.E. Brodley, and T.A. Trikalinos. Class imbalance, redux. In *Proc. ICDM*, 2011. [7](#)
- [62] Z. Wang and J. Ye. Querying discriminative and representative samples for batch mode active learning. *ACM Trans. Knowl. Discov. Data*, 2015. [3](#)
- [63] K. Wei, R. Iyer, and J. Bilmes. Submodularity in data subset selection and active learning. In *ICML*, 2015. [2](#)
- [64] Gert W. Wolf. Facility location: Concepts, models, algorithms and case studies. series: Contributions to management science. 2011. [2](#)
- [65] H. Zhang, M. Cissé, Y. N. Dauphin, and D. Lopez-Paz. mixup: Beyond empirical risk minimization. *CoRR*, 2017. [7](#)
- [66] Yuxun Zhou and Costas J. Spanos. Causal meets submodular: Subset selection with directed information. In *Proceedings of the 30th International Conference on Neural Information Processing Systems, NIPS'16*, page 2657–2665, 2016. [2](#)

Appendix

Lemma 1. *The function $f_{\text{diversity}}$ is monotonically non-decreasing and submodular.*

Proof. The function $f_{\text{diversity}}$ is given by

$$f_{\text{diversity}}(S) = \sum_{i \in S} \max_{l \in G} \sum_{j: (l,j) \in E} s(l,j) - \gamma \sum_{i,j: (i,j) \in E, i,j \in S} s(i,j). \quad (13)$$

We will show that the function is monotonically non-decreasing and submodular when $0 \leq \gamma \leq 1$.

We will first show that the function is monotonically non-decreasing. Consider an element $e \in G \setminus S$:

$$f_{\text{diversity}}(S \cup e) - f_{\text{diversity}}(S) = \max_{l \in G} \sum_{j: (l,j) \in E} s(l,j) - \gamma \sum_{j: (e,j) \in E, j \in S} s(e,j) \quad (14)$$

In the first term, $j \in G$, whereas in the second $j \in S$. The first term is a maximum over all samples in G , including $l = e$. Since $\lambda \leq 1$ and $S \subseteq G$, we have $f_{\text{diversity}}(S \cup e) - f_{\text{diversity}}(S) \geq 0$ and thus the function in Eq. 13 is monotonically non-decreasing.

Next, we will show that the function $f_{\text{diversity}}(S)$ is submodular. In order to do this, we show the following when $A, B \subseteq G$, $B \subseteq A$, and $e \in G \setminus A$:

$$f_{\text{diversity}}(A \cup e) - f_{\text{diversity}}(A) \leq f_{\text{diversity}}(B \cup e) - f_{\text{diversity}}(B) \quad (15)$$

We expand the left hand side of the above expression using the definition of $f_{\text{diversity}}(S)$:

$$f_{\text{diversity}}(A \cup e) - f_{\text{diversity}}(A) = \max_{l \in G} \sum_{j: (l,j) \in E} s(l,j) - \lambda \sum_{j: (e,j) \in E, j \in A} s(e,j) \quad (16)$$

We expand the right hand side as follows:

$$f_{\text{diversity}}(B \cup e) - f_{\text{diversity}}(B) = \max_{l \in G} \sum_{j: (l,j) \in E} s(l,j) - \gamma \sum_{j: (e,j) \in E, j \in B} s(e,j) \quad (17)$$

Subtracting Eq. 17 from Eq. 16 we have:

$$\begin{aligned} (f_{\text{diversity}}(A \cup e) - f_{\text{diversity}}(A)) - (f_{\text{diversity}}(B \cup e) - f_{\text{diversity}}(B)) &= \\ \gamma \sum_{j: (e,j) \in E, j \in B} s(e,j) - \gamma \sum_{j: (e,j) \in E, j \in A} s(e,j) &= \end{aligned} \quad (18)$$

Since $\gamma \geq 0$, $s(\cdot, \cdot) \geq 0$, and $B \subseteq A$, we satisfy Eq. 15. \square

Lemma 2. *The function f_{triple} is monotonically non-decreasing and submodular.*

Proof. The function f_{triple} is given by

$$f_{\text{triple}}(S) = \sum_{i \in S} \alpha(i) - \eta \sum_{i,j,k: (i,j,k) \in \mathcal{T}, i,j,k \in S} t(i,j,k). \quad (19)$$

We will show that the function is monotonically non-decreasing and submodular when $0 \leq \eta \leq 1$.

We will first show that the function is monotonically non-decreasing. Consider an element $e \in G \setminus S$:

$$f_{\text{triple}}(S \cup e) - f_{\text{triple}}(S) = \alpha(e) - \eta \sum_{e,j,k: (e,j,k) \in \mathcal{T}, e,j,k \in S} t(e,j,k) \quad (20)$$

The first term $\alpha(e)$ is the number of triple cliques associated with e , and the maximum value of the second term is $\alpha(e)$ since $0 \leq \eta \leq 1$. Thus we have $f_{\text{triple}}(S \cup e) - f_{\text{triple}}(S) \geq 0$ and thus the function in Eq. 19 is monotonically non-decreasing.

Next, we will show that the function $f_{\text{triple}}(S)$ is submodular. In order to do this, we show the following when $A, B \subseteq G$, $B \subseteq A$, and $e \in G \setminus A$:

$$f_{\text{triple}}(A \cup e) - f_{\text{triple}}(A) \leq f_{\text{triple}}(B \cup e) - f_{\text{triple}}(B) \quad (21)$$

We expand the left hand side of the above expression using the definition of $f_{\text{triple}}(S)$:

$$f_{\text{triple}}(A \cup e) - f_{\text{triple}}(A) = \alpha(e) - \eta \sum_{e,j,k: (e,j,k) \in \mathcal{T}, e,j,k \in A} t(e,j,k) \quad (22)$$

We expand the right hand side as follows:

$$f_{\text{triple}}(B \cup e) - f_{\text{triple}}(B) = \alpha(e) - \eta \sum_{e,j,k: (e,j,k) \in \mathcal{T}, e,j,k \in B} t(e,j,k) \quad (23)$$

Subtracting Eq. 23 from Eq. 22 we have:

$$\begin{aligned} & (f_{\text{triple}}(A \cup e) - f_{\text{triple}}(A)) - \\ & (f_{\text{triple}}(B \cup e) - f_{\text{triple}}(B)) = \\ & \eta \sum_{e,j,k: (e,j,k) \in \mathcal{T}, e,j,k \in B} t(e,j,k) - \end{aligned} \quad (24)$$

$$\eta \sum_{e,j,k: (e,j,k) \in \mathcal{T}, e,j,k \in A} t(e,j,k) \quad (25)$$

Since $\eta \geq 0$, $t(\cdot, \cdot, \cdot) \geq 0$, and $B \subseteq A$, we satisfy Eq. 21. \square

Lemma 3. *The function f_{mmd} is monotonically non-decreasing and submodular.*

Proof. f_{mmd} is defined as

$$f_{\text{mmd}}(S) = \sum_{i \in S} \sum_{j: (i,j) \in E, j \in G} s(i,j) - \xi \sum_{i,j: (i,j) \in E, i,j \in S} s(i,j). \quad (26)$$

Under the condition $0 \leq \xi \leq 1$, we will first show that the function is monotonic, and then prove the submodularity condition.

Let us consider the marginal gain while adding an element $e \in G \setminus S$:

$$\begin{aligned} f_{\text{mmd}}(S \cup e) - f_{\text{mmd}}(S) &= \sum_{j: (e,j) \in E, j \in G} s(e,j) - \\ & \xi \sum_{j: (e,j) \in E, j \in S} s(e,j) \end{aligned} \quad (27)$$

Since $\xi \leq 1$ and $S \subseteq G$, we have $f_{\text{mmd}}(S \cup e) - f_{\text{mmd}}(S) \geq 0$ and thus the function in Eq. 26 is monotonically non-decreasing.

To prove that $f_{\text{mmd}}(S)$ is submodular, we show the following when $A, B \subseteq G$, $B \subseteq A$, and $e \in G \setminus A$:

$$f_{\text{mmd}}(A \cup e) - f_{\text{mmd}}(A) \leq f_{\text{mmd}}(B \cup e) - f_{\text{mmd}}(B) \quad (28)$$

We rewrite the left hand side of the above expression using the definition of $f_{\text{mmd}}(S)$:

$$\begin{aligned} f_{\text{mmd}}(A \cup e) - f_{\text{mmd}}(A) &= \sum_{j: (e,j) \in E, j \in G} s(e,j) - \\ & \xi \sum_{j: (e,j) \in E, j \in A} s(e,j) \end{aligned} \quad (29)$$

Now we express the right hand side as follows:

$$\begin{aligned} f_{\text{mmd}}(B \cup e) - f_{\text{mmd}}(B) &= \sum_{j: (e,j) \in E, j \in G} s(e,j) - \\ & \xi \sum_{j: (e,j) \in E, j \in B} s(e,j) \end{aligned} \quad (30)$$

Subtracting Eq. 30 from Eq. 29 we have:

$$\begin{aligned} & (f_{\text{mmd}}(A \cup e) - f_{\text{mmd}}(A)) - \\ & (f_{\text{mmd}}(B \cup e) - f_{\text{mmd}}(B)) = \\ & \xi \sum_{j: (e,j) \in E, j \in B} s(e,j) - \xi \sum_{j: (e,j) \in E, j \in A} s(e,j) \leq 0. \end{aligned} \quad (31)$$

The inequality holds since $\xi \geq 0$, $s(\cdot, \cdot) \geq 0$, and $B \subseteq A$. This implies that Eq. 28 is true. \square